Proceedings of ISFOG 2025
5TH INTERNATIONAL SYMPOSIUM ON
FRONTIERS IN OFFSHORE GEOTECHNICS
Nantes, France | June 9-13 2025

ISBN 978-2-85782-758-0

Definition of primary and unloading / reloading stiffness curves to model lateral monopile behaviour for design of offshore structures

L. Berenguer Todo Bom*
COWI A/S, Hamburg, Germany

C. Quirante
COWI A/S, Hamburg, Germany

**lbbm@cowi.com (corresponding author)*

ABSTRACT: The dimensions of offshore monopile foundations are mainly governed by lateral performance, namely the lateral strength and irrecoverable rotation design criteria. Numerical modelling of environmental loading applied to the foundation relies on the definition of soil interaction stiffness curves to derive foundation strength and deformability. The determination of the primary/virgin loading stiffness curve of monopiles under lateral loading has been subject of numerous studies, notably the PISA design approach, supported by finite element (FE) modelling. However, in new geographies and during earlier stages of design, numerical analyses are cumbersome hence an alternative approach to derive rule-based components of the PISA methodology is needed. Moreover, the unloading stiffness is still conservatively assumed in design practice as the initial stiffness, resulting in an overestimation of the permanent rotation caused by extreme wave loading. The determination of the unloading and reloading lateral stiffness can have significant influence on the design of large diameter monopile structures. This article presents a methodology to define both the primary and unloading/reloading lateral monopile curve. The primary loading curve is defined based on a rule-based approach, formulated in total stress space, which adopts the fundamental principles of soil mechanics to match the soil spring data from finite element models. The unloading/reloading lateral behavior of the monopile is modeled using a hysteretic soil damping curve derived from analytical methods, based on the intrinsic relationship between the two physical quantities. The stiffness curves developed through this methodology are benchmarked against results from 3D FE analyses based on typical North Sea conditions.

Keywords: PISA methodology, finite element modelling, monopiles, damping, unloading stiffness

1 INTRODUCTION

The monopile structure is the most common foundation type supporting offshore wind turbine generators (WTG) worldwide. This dominance continues to grow as advancements in monopile modeling techniques enable more optimized designs, and the fabrication, transportation, and installation of larger diameter monopiles become feasible, allowing this foundation to carry ever greater loads from large WTG structures.

The design requirements influencing monopile geometry are primarily driven by lateral performance, specifically lateral resistance and irrecoverable deformation, which correspond to ultimate and serviceability limit states, respectively. These verifications depend on both the design loads and the lateral soil interaction stiffness curves. The influence of the soil stiffness is twofold, both as a resistance component but also on the design loads since these are inversely correlated, due to the dynamic nature of loading in offshore wind structures.

The complete definition of the lateral soil interaction stiffness comprises both the primary/virgin and the unloading/reloading backbone curve. The PISA design methodology by Byrne et al. (2017) provides a framework to derive the primary/virgin loading stiffness curve, either through an analytical rule-based approach or based on the finite element method (FEM). Concerning the unloading and reloading lateral stiffness behaviour, however, in spite of its relevance, is often overlooked in geotechnical modelling integrated load analysis (ILA) and geotechnical design verifications.

This paper presents a design approach to derive both the primary/virgin and the unloading/reloading lateral backbone curves for monopile structures adopting analytical formulations. The proposed methodologies are benchmarked to numerical solutions using the FEM and typical soil conditions in the North Sea. Based on the findings, recommendations are provided to guide designers during early and detailed phases of monopile design.

2 ADAPTED RULE-BASED APPROACH

The iterative design process for offshore wind structures, given its multidisciplinary nature, demands robust geotechnical modeling approaches that are computationally efficient while maintaining accuracy comparable to finite element (FE) models. These simplified models typically adopt a 1D Beam-in-Elastic Foundation (BEF), resorting to soil-structure interaction models consisting of non-linear interaction curves. The definition of the non-linear interaction curves can be based on FE models or analytical rule-based approaches. The PISA rule-based design model (Burd et al., 2020), calibrated on pile load tests at specific sites, defines the soil curves in non-dimensional space with a normalization approach encompassing soil properties and—pile geometry. Alternatively, Jeanjean and Zakeri (2023) proposed a site-independent rule-based methodology based in soil mechanics principles for resistance components, employing the direct simple shear stress-strain curve as reference to define the initial stiffness and curve shapes. The benefits of both approaches, site-independent formulation and curve definition in normalized space, together with further calibration against a database of FE-calibrated PISA parameters, provides a valuable tool for designers.

A proposed rule-based approach and the references considered in its derivation is given in Table 1. This approach is further complemented by experience-based multipliers and deltas given in Table 2. Lower bound values are provided to account for sites with high stiffness contrasts in layered soils where rule-based approaches tend to underperform (Burd et al., 2020). The values therein should be multiplied by those obtained in Table 1, except for the n curvature parameters where they where they are additive and referred to as deltas. These multipliers and deltas are informed by a large database of previous XXL monopile designs performed in the commercial software PLAXIS using the NGI-ADP total stress model. The values provided in Table 2 are determined from statistical analyses of the ratios between calibrated PISA parameters, derived from FEM analyses, and the respective analytical equations as given in Table 1. An example of such an assessment for the PISA multiplier of the ultimate lateral resistance is shown in Figure 1. The proposed rule-based approach is defined in total stress space and adopts the fundamental principles of soil mechanics to match the soil spring data obtained from multiple FE models across various sites. Site-specific calibration of the multipliers and deltas can be achieved by carrying out a limited number of FE model simulations to determine global PISA parameters.

Table 1. Normalized parameters in total stress

PISA		Equation / Value	Reference
$\boldsymbol{p-v}$	$\bar{v}_{pu}$	$5\% \cdot G_0/S_u$	(Jeanjean and Zakeri, 2023)
	k_p	4.5	(Suryasentana and Lehane, 2016)
	n_p	0.85	(Darendeli, 2001)
	$\bar{p}_u$	$N_p \leq N_{pd}$ $N_{pd} = 9 + 3\alpha$	(Jeanjean et. al, 2017)
$\boldsymbol{m-\theta}$	$\bar{\psi}_{mu}$	$\bar{m}_u/k_m$	(Burd et al., 2020)
	k_m	$\alpha/0.45$	(Jeanjean and Zakeri, 2023)
	n_m	0.25	(Burd et al., 2020)
	$\bar{m}_u$	α	(Jeanjean and Zakeri, 2023)
$\boldsymbol{H_B-v_B}$	$\bar{v}_{Hu}$	$\bar{H}_{Bu}/k_H$	-
	k_H	$\pi/0.84$	(Jeanjean and Zakeri, 2023)
	n_H	0.15	-
	$\bar{H}_{Bu}$	$\pi/4$	(Jeanjean and Zakeri, 2023)
$\boldsymbol{M_B-\theta_B}$	$\bar{\psi}_{Mu}$	$\bar{M}_{Bu}/k_M$	-
	k_M	$\pi/2.91$	(Jeanjean and Zakeri, 2023)
	n_M	0.40	-
	$\bar{M}_{Bu}$	$\pi/6$	(Jeanjean and Zakeri, 2023)

Table 2. Multipliers and deltas of PISA parameters

Soil curves	PISA	$\boldsymbol{M_{PISA}}$ / $\boldsymbol{\Delta_{PISA}}$	
		Best	**Lower**
$\boldsymbol{p-v}$	$\bar{v}_{pu}$	0.24	0.24
	k_p	2.10	1.50
	n_p	-0.25	-0.25
	$\bar{p}_u$	1.20	1.00
$\boldsymbol{m-\theta}$	$\bar{\psi}_{mu}$	2.00	2.00
	k_m	0.29	0.29
	n_m	0.00	0.00
	$\bar{m}_u$	0.90	0.71
$\boldsymbol{H_B}$-$\boldsymbol{v_B}$	$\bar{v}_{Hu}$	20.0	20.0
	k_H	0.13	0.13
	n_H	0.00	0.00
	$\bar{H}_{Bu}$	0.38	0.38
$\boldsymbol{M_B}$-$\boldsymbol{\theta_B}$	$\bar{\psi}_{Mu}$	40.0	40.0
	k_M	0.14	0.14
	n_M	0.00	0.00
	$\bar{M}_{Bu}$	0.83	0.83

Finally, drainage assessments of coarse-grained materials for large diameter monopiles do not indicate fully drained behaviour (Osman and Randolph, 2012). Hence, total stress approaches are a pragmatic approach to extend the PISA formulation to the undrained loading of sands (Berenguer Todo Bom, 2024).

The primary/virgin backbone curve of the monopile foundation can be directly obtained from the equations provided in conjunction with the PISA clay framework.

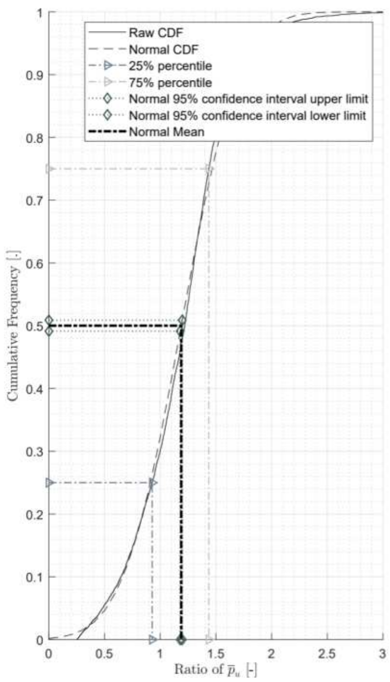

Figure 1. Cumulative distribution function (CDF) of multiplier of $\bar{p}_u$

3 UNLOADING AND RELOADING LATERAL STIFFNESS

The determination of the unloading and reloading stiffness has received considerably less attention in offshore geotechnical engineering research, compared to the field of earthquake geotechnical engineering. The extended Masing rules (Masing, 1926) remain a commonly used approach to define the unloading/reloading stress–strain loops. The hysteretic damping ratio under the Masing rules, however, which is a direct function of the unloading/reloading behaviour, is overestimated at the medium to large strain range. The determination of the unloading/reloading stiffness curve can be obtained from the primary backbone curve and hysteretic damping curve. In the following sections the mathematical formulation of a 1D model able to capture this behaviour is presented and later used to demonstrate its ability to define the unloading/reloading backbone curve.

3.1 1D Model description

The analytical ‘backbone’ curve formulation is based on the Generalized Quadratic/Hyperbolic (GQ/H) Model with Shear Strength Control (Groholski et al., 2016), which is defined by the force-displacement, $F - u$, curve as follows:

$$F = F_{max} \left[\frac{1}{2\,\theta_F} \left\{ 1 + \left(\frac{u}{u_r}\right) - \sqrt{\left\{ 1 + \left(\frac{u}{u_r}\right) \right\}^2 - 4\,\theta_F \left(\frac{u}{u_r}\right)} \right\} \right] \tag{1}$$

where the θ_F variable is a curve fitting parameter and the reference displacement is defined as $u_r = \frac{F_{max}}{K_0}$, where F_{max} refers to the maximum force and K_0 the initial pile stiffness. The unloading/reloading curve formulation, including a reduction factor according to the MRDF approach (Phillips and Hashash, 2009) to better match the damping curve, can be obtained by modifying the second Masing rule based on the backbone equation (Groholski et al., 2016).

3.2 Damping curve

The damping ratio curve is a necessary input to determine the unloading/reloading backbone curve (Markou and Kaynia, 2018). This section outlines two methods for determining the equivalent hysteretic damping ratio curve: one based on the 1D BEF and a second on FE models.

3.2.1 1D BEF model

The procedure to determine the damping curve is partially illustrated in Figure 2. For each cyclic displacement level, the deformed shape of the pile can be obtained from the primary backbone curve. The shear strain γ relationship to displacement u, where υ is the Poisson ration and D the pile diameter, provided by Skempton (1951) allows the determination of the dissipated E_D and stored energy E_S components per depth as follows:

$$\gamma(z) = \frac{1+\upsilon}{2.5\,D}\, u(z) \tag{2}$$

$$E_{S(z)} = 0.5\, G_{eq(z)}\, \gamma^2(z) \tag{3}$$

$$E_{D(z)} = 4\pi\, E_{S(z)}\, \xi_{eq}(z) \tag{4}$$

The global equivalent hysteretic damping ratio curve can be determined by simple integration of the energy components along the depth of the pile down to the pile tip as follows:

$$\xi_{eq-1D} = \frac{\int_0^L E_{D(z)}\,dz}{4\pi \int_0^L E_{S(z)}\,dz} \tag{5}$$

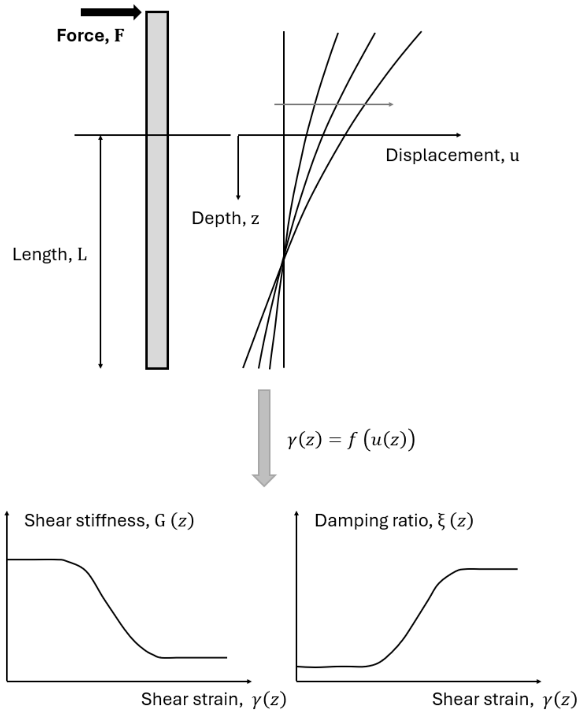

Figure 2. Damping ratio curve from 1D-BEF model

3.2.2 Finite element model

The use of macro-element models for the behaviour of monopile foundations is a common design approach (Kaynia, 2018). This simplifies the modelling of unloading/reloading behaviour since complex local phenomena, e.g., gapping, can be captured in FE models included in the macro-element implicitly. To determine the damping ratio curve, several one-way cycles of increasing amplitude are modelled in FE, Figure 3. The methodology is also be applicable to low amplitude two-way cyclic loading. It should be noted that complex phenomena such as large gapping and non-negligible suction behind the pile may occur in such loading cases, where simple analytical approaches may not suffice and for which FEM remains the most adequate modelling approach.

The hysteretic damping is proportional to the dissipated energy per cycle hence proportional to the area generated by the unloading/reloading hysteretic loop. From the FE model, therefore, the foundation equivalent hysteretic damping ratio is computed as follows, where E_D is the global dissipated energy in a full hysteresis and E_S is the global elastic strain energy.

$$\xi_{eq-FE} = \frac{1}{4\pi}\frac{E_D}{E_S} \tag{6}$$

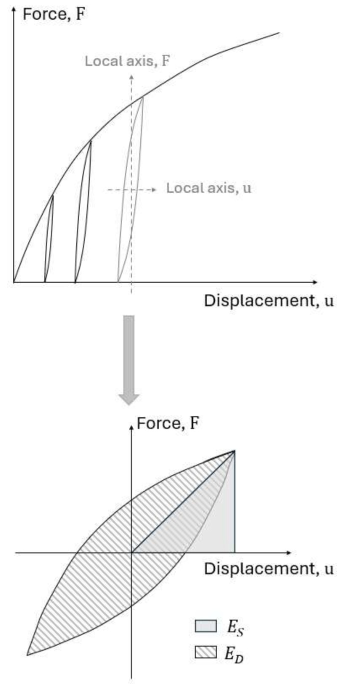

Figure 3. Damping ratio curve from FE model

4 FINITE ELEMENT ANALYSIS

Three finite element (FE) models of a monopile foundation using PLAXIS 3D are undertaken to perform sensitivity studies of the proposed approaches based on typical North Sea conditions. The FE monopiles are laterally loaded both monotonically and cyclically to determine the load-displacement behaviour at mudline. The effects of cyclic degradation are not considered in this study. The interface formulation in the FE model imposes a gapping condition to avoid tension forces developing at the back of the monopile. The pile is modelled as a linear elastic element using plate elements with a Young’s modulus of 210 GPa and a Poisson ratio of 0.3. The pile geometrical properties consist of a diameter of 10m and wall thickness of 85mm. A prescribed displacement is applied at a height of 45 m above the mudline to maintain a constant ratio between shear force and moment at the mudline.

4.1 Soil profiles and parameters

The soil parameters and models used in both the 1D-BEF and FE models are presented in Figure 4, Table 3 and Table 4.

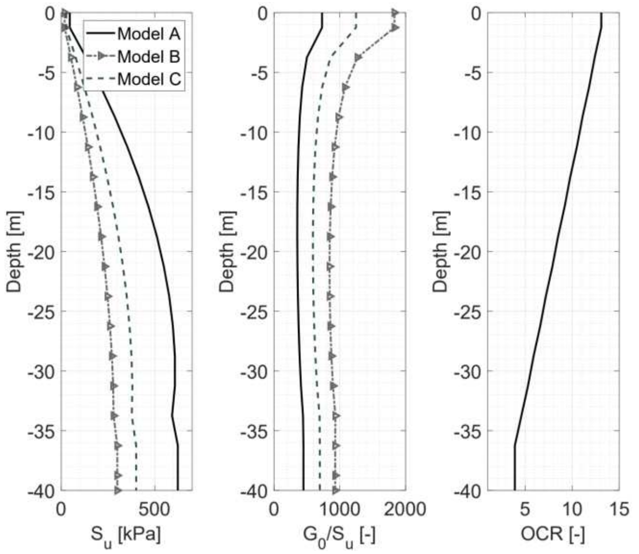

Figure 4. Total stress models – Soil inputs

An additional effective-stress model is also considered as benchmark, comparable to Model A as per equivalence shown in Berenguer Todo Bom (2024). This choice is made because the HSsmall model more accurately captures unloading/reloading behavior compared to the NGI-ADP model. For any parameter values not provided explicitly, the PLAXIS default value is adopted.

Table 3. Soil parameters of HSsmall model

HSsmall	Units	Value
$\boldsymbol{\varphi}$	[°]	42
E_{50}^{ref}	[MPa]	60
E_{oed}^{ref}	[MPa]	60
E_{ur}^{ref}	[MPa]	180
m	[-]	0.5
p^{ref}	[kPa]	100
G_0^{ref}	[MPa]	130
$\gamma_{0.7}$	[%]	0.0246

Table 4. Soil parameters of NGI-ADP models

NGI-ADP	Units	Cases analysed		
		Model A	Model B	Model C
γ_f^C	[%]	5	5	5
γ_f^E	[%]	10	10	10
γ_f^{DSS}	[%]	7.5	7.5	7.5
$\frac{S_u^p}{S_u^A}$	[-]	0.70	0.86	0.77
$\frac{S_u^{DSS}}{S_u^A}$	[-]	0.85	0.93	0.89
$\frac{\tau_0}{S_u^A}$	[-]	0.0	0.0	0.0

4.2 Results and comparison

The monotonic load-displacement curve of the 1D-BEF and FE models as well as the pile lateral stiffnesses K_{pile}, determined as the ratio between the shear force and horizontal displacement at mudline, are presented in Figure 5. The adapted rule-based approach provides a good match to the FE models while remaining an adequately conservative estimate. As anticipated, the drained ultimate capacity is underestimated in the total stress modeling, primarily due to the exclusion of the frictional contribution from increased horizontal stress during loading. This difference in pile response is typically only observed at very high load levels, which are beyond practical engineering considerations.

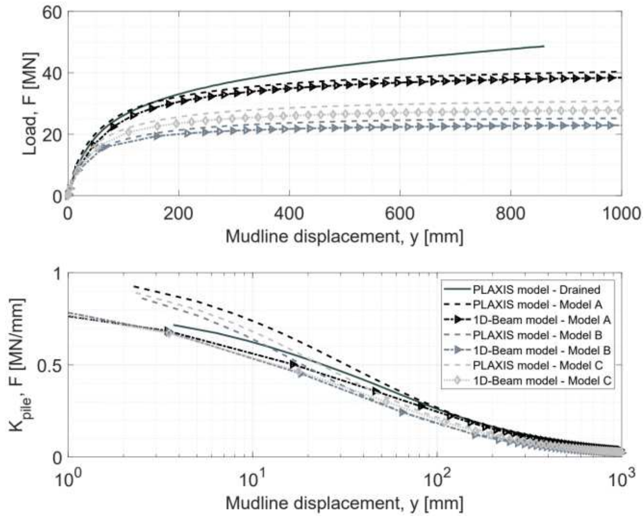

Figure 5. Primary/virgin backbone curves

The damping ratio curves determined according to the methodologies detailed in the previous sections, for both the 1D-BEF and FE model, are shown in Figure 6. Despite the linear unloading/reloading in the NGI-ADP constitutive model, and the ability of the HSsmall model to capture the hysteretic loops, a relatively good agreement is observed between the FE models. The damping ratio curve derived from the 1D-BEF model approach detailed in section 3.2.1, underestimates damping compared to the FE models. The discrepancy is likely due to the non-inclusion of the gapping behaviour and and the fact that the damping in the 1D-BEF approach is derived solely from the interaction of the p-y curves, neglecting other soil-structure interaction effects.

Based on the primary backbone and hysteretic damping ratio curves, the unloading/reloading backbone curves can be derived adopting the 1D GQ/H analytical model and compared to the results obtained from the PLAXIS FE models. The calibrated parameters of the GQ/H model are provided in Table 5, including those for the modulus reduction MRDF approach (Phillips and Hashash, 2009). The $\boldsymbol{\theta}$ and $\boldsymbol{p}$ parameters provided in Table 5, are curve fitting parameters, as per the formulation of the backbone curve and unloading/reloading behaviour of the analytical model detailed in Groholski et al. (2016). As shown in Figure 7, the FE unloading/reloading backbone is characterized by a less pronounced stiffness reduction with increasing strain compared to the primary/virgin backbone curve. These results are consistent with the Masing-based curves derived from the calibrated GQ/H models, aligning with both the FEM results and the calibrated 1D-BEF rule-based monopile model.. Moreover, as known in Masing unloading/reloading rules, the damping ratio is overestimated at large displacements.

The models A, B and C indicate similar results, therefore solely model C is investigated in further detail to limit the number of curves analysed. The results obtained for model C are shown in Figure 7 which include the FEM, fitted analytical model to both FEM and 1D-BEF and a non-Masing calibrated GQ/H model to the 1D-BEF model.

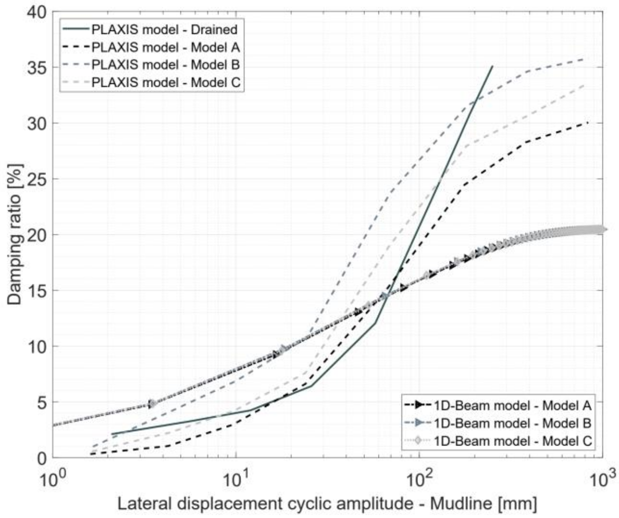

Figure 6. Equivalent hysteretic damping ratio curves

The ability to better match the damping using the MRDF approach, deviating from Masing's principles resulting in slimmer hysteresis loops has the drawback that the unloading stiffness can be lower than the loading stiffness. For the selection of macro-models to be used in integrated load analyses (ILA), the ability to match the unloading/reloading stiffness and damping behaviour observed in FEM is an advantage. Matching both for different magnitudes of strain ranges is, however, not practical due to the required complexity of models. A pragmatic approach, based on the results presented, could involve applying Masing's principles for small strain ranges, such as in fatigue load cases. For medium to large strain ranges, such as ultimate limit state cases, priority should be given to not overestimating damping levels to avoid underestimating the design loads and hence non-Masing approaches should be adopted.

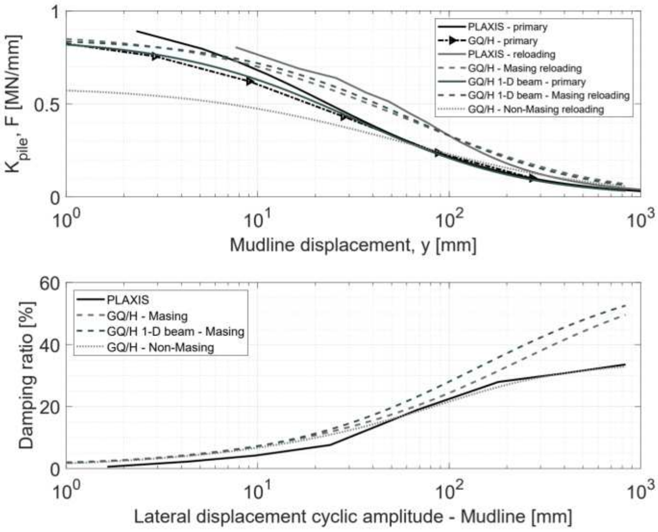

Figure 7. Primary/virgin backbone curves

Table 5. GQ/H parameters – FE and Model C

GQ/H model	Units	FE	1D BEF
$\boldsymbol{F_{max}}$	[MN]	31.3	27.8
$\boldsymbol{K_0}$	[MN/mm]	0.878	0.852
$\boldsymbol{\xi_{min}}$	[%]	0.55	1.14
$\boldsymbol{\theta_1}$	[-]	-4.69	-0.43
$\boldsymbol{\theta_2}$	[-]	8.21	0.61
$\boldsymbol{\theta_5}$	[-]	0.11	0.50
$\boldsymbol{P_1}$	[-]	0.92	-
$\boldsymbol{P_2}$	[-]	0.37	-
$\boldsymbol{P_3}$	[-]	8.17	-

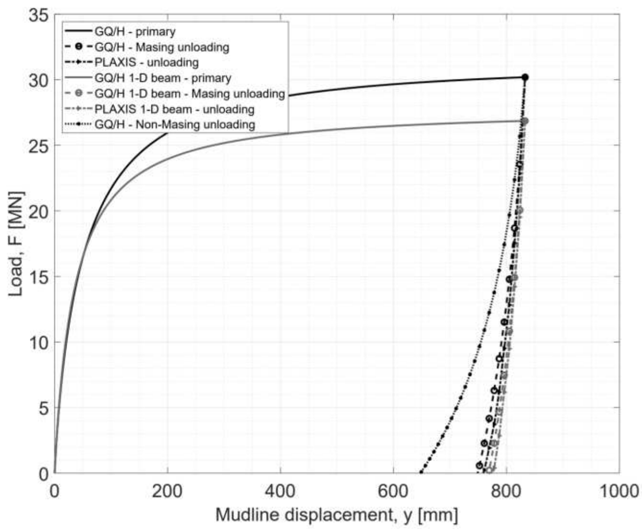

Figure 8. Unloading-reloading load-displacement curves

Finally, caution is also advised when selecting the unloading backbone curve to verify the permanent rotation criterion. This is exemplified in Figure 8, where the lower damping curve fitting to match the FE results calculates a non-conservative permanent rotation. The Masing unloading backbone curve, calibrated to either the FE or 1D BEF damping curves, provides very similar results to the FE models despite the large displacement range and seems to indicate that it is reasonable to be used in design verification of permanent rotation.

5 CONCLUSIONS

The formulations to derive the primary and unloading/reloading stiffness backbone curves of monopile foundations have been presented. The method to obtain the unloading/reloading backbone curve supported on the hysteretic damping, from either a FE or 1D BEF model, has been detailed. A comparison to FEM results indicates the rule-based approach proposed to be adequately conservative and that the Masing calibrated GQ/H model can reproduce the lateral unloading stiffness behaviour of the FE models. The analytical GQ/H model is not able to both match damping and unloading/reloading stiffness at all strain ranges in ILA calculations. Therefore, it is recommended that solely for the small strain range the Masing's principles be adopted while for large strain range priority be given to matching the damping ratio accurately. Finally, for the determination of permanent rotation, the better match with FEM in this paper is found when adopting a Masing unloading backbone curve. This may not always be the case as it depends on the load level and hence it is recommended that the most conservative of either options, Masing or non-Masing unloading stiffness, be adopted for the estimation of the permanent rotation.

AUTHOR CONTRIBUTION STATEMENT

First Author: Conceptualization, Methodology, Formal Analysis, Writing- Original draft. **Other Author**.: Data curation, Reviewing and Editing.

REFERENCES

Berenguer Todo Bom (2024). Generalized P-y curves for monopile design using the PISA methodology. ECSMGE - XVIII European Conference on Soil Mechanics and Geotechnical Engineering.

Burd et al. (2020). PISA: Application of the PISA design model to monopiles embedded in layered soils, Géotechnique 2020 70:11, 1067-1082. https://doi.org/10.1680/jgeot.20.PISA.009.

Byrne et al. (2017). PISA: New Design Methods for Offshore Wind Turbine Monopiles. Proc. 8th Int. Conf. for Offshore Site Investigation and Geotechnics, London.

Darendeli, M. B. (2001). "Development of a New Family of Normalized Modulus Reduction and Material Damping Curves", Austin, Texas.

Groholski, D., Hashash, Y., Kim, B., Musgrove, M., Harmon, J., and Stewart, J. (2016). "Simplified Model for Small-Strain Nonlinearity and Strength in 1D Seismic Site Response Analysis." J. Geotech. Geoenviron. Eng.

Jeanjean et al. (2017). A framework for monotonic p-y curves in clays. In Offshore Site Investigation Geotechnics 8th International Conference Proceeding (Vol. 108, No. 141, pp. 108-141). Society for Underwater Technology.

Jeanjean, P. and Zakeri A. (2023). Efficiencies and challenges in offshore wind foundation design. In Offshore Site Investigation Geotechnics 9th International Conference Proceeding (Vol. 109, pp. 700-141). Society for Underwater Technology.

Jindal, S., Rahmanli, U., Aleem, M., Cui, L., Jalbi, S. and Bhattacharya, S. (2024). Identification of soil damping for stiff piles based on experiments: Methodology and results. Ocean Engineering. 301. 10.1016/j.oceaneng.2024.117124.

Kaynia, A. (2018). Seismic considerations in design of offshore wind turbines. Soil Dynamics and Earthquake Engineering. 124. 399-407. 10.1016/j.soildyn.2018.04.038.

Markou A., Kaynia A. (2018). Nonlinear soil-pile interaction for offshore wind turbines. Wind Energy. http://dx.doi.org/10.1002/we.2178.

Masing, G. (1926). "Eigenspannungen und Verfestigung beim Messing." 2nd Int. Congress on Applied Mechanics, Orell FüssliZurich, Switzerland.

Osman, A. S., & Randolph, M. F. (2012). Analytical Solution for the Consolidation around a Laterally Loaded Pile. International Journal of Geomechanics, 12(3), 199–208. doi: 10.1061/(asce)gm.1943-5622.0000123

Phillips, C. and Hashash, Y. (2009) "Damping formulation for non-linear 1D site response analyses" Soil Dynamics and Earthquake Engineering, v. 29, pp 1143–1158.

PLAXIS 3D Material Models Manual (2023).

Skempton, A. W. (1951) : The bearing capacity of clays. Building Research Congress, Division 1, Part 3, London, pp. 180-189.

Suryasentana, S. and Lehane, B. (2016). Updated CPT-based p – y formulation for laterally loaded piles in cohesionless soil under static loading. Géotechnique. 66. 1-9.